Enhancing the sensitivity of a high resolution negative-tone metal organic photoresist for extreme ultra violet lithography

Scott M. Lewis*[a&d], Hayden R. Alty[b], Michaela Vockenhuber[c], Guy A. DeRose[a], Dimitrios Kazazis[c], Grigore A. Timco[b], James A. Mann[b], Paul Winpenny[d], Axel Scherer[a], Yasin Ekinci[c], Richard Winpenny[b&d]

[a]Dept. of Applied Physics and Material Science, California Institute of Technology, 1200 East California Boulevard, MC 200-79, Pasadena, 91125 CA, USA;

[b]Dept. of Chemistry and photon science institute, The University of Manchester, Oxford Road, Manchester, M13 9PL, UK;

[c]Advanced Lithography and Metrology Group, Paul Scherrer Institute, Forschungsstrasse 111, 5232 Villigen, Switzerland;

[d]Sci-Tron Ltd, 34 High Street, Aldridge, Walsall, WS9 8LZ, UK.

Abstract

In this paper, we report on a novel metal organic photoresist based on heterometallic rings that was designed for electron beam and extreme ultraviolet lithography. From initial electron beam lithography studies, the resist performance demonstrated excellent resolution of 15 nm half-pitch (HP) and a silicon dry etch selectivity of 100:1 but at the expense of sensitivity. To improve sensitivity, a 3D Monte Carlo simulation was employed that utilizes a secondary electron generation model. The simulation suggested that the sensitivity could be dramatically improved while maintaining high resolution by incorporating $HgCl_2$ species into the resist molecular design. This considerably improved the resist sensitivity without losing the high resolution, where it was determined that the resist sensitivity was increased by a factor of 1.6 and 1.94 while demonstrating a resolution of 15 nm and 16 nm HP when exposed with electrons and EUV radiation respectively. Using x-ray photoelectron spectroscopy measurements, we show that after exposure to the electron beam the resist materials are transformed into a metal oxyfluoride and this is why the resist demonstrates high resistance to silicon dry etch conditions achieving a selectivity of 60:1 at a resolution of 15 nm HP.

Keywords: Metal Organic EUV photoresist, Metal Organic electron beam resist, extreme ultra violet lithography, electron beam lithography, Excalibur Monte Carlo Simulation

1. INTRODUCTION

Modern society is driven by the electronics industry. The electronic industry manufactures electronic devices that contain integrated circuits (IC), where the crucial component of those ICs are field-effect transistors (FETs). Manufacturing these FETs relies upon a technique called photolithography. By changing the light source to shorter wavelengths it is possible to fabricate their next generation products with ever smaller features than the previous generation. Over the last fifty years, the electronics industry have been able to follow a trend known as "Moore's Law" to reduce the size of the FETs by a factor of two every two years. The electronics industry follows a roadmap that assumes that this constant reduction of size will continue – at least until the mid-2020s [1]. Today extreme ultraviolet lithography (EUVL) (where the wavelength is 13.4 nm) is employed to manufacture the latest GAAFET (Gate All Around FET) for the 5 nm node, these devices are multi-gate FETs where the gates wrap around fin-like channels. Going beyond the 5 nm node, it is evident that producing the next generation nanopatterns can be fabricated using the EUVL technology, but unfortunately, it will become increasingly challenging to transfer the patterns into the silicon with existing organic resist materials. This is due to the aggressive conditions of the etch plasma. As the feature size of the FETs decreases below 20 nm, the plasma particle density will need to be increased substantially. This inherently leads to a decrease in etch efficiency [2, 3]. To alleviate this issue, inorganic resist materials must be explored because they have been found to provide superior etch selectivity.

Previously, we have shown a negative-tone metal-organic resist that produced line and space patterns of 20 nm half-pitch (HP) resolution [2]. The resolution that we reported was produced at the expense of resist sensitivity, where

Advances in Patterning Materials and Processes XL, edited by Douglas Guerrero, Gilles R. Amblard, Proc. of SPIE Vol. 12498, 124980X · © 2023 SPIE
0277-786X · doi: 10.1117/12.2658324

the exposure dose was 61000 μC/cm^2 for electron beam lithography (EBL). Even though the resist sensitivity is poor, it showed great potential as it demonstrated an extraordinary silicon dry etch performance of > 100:1 selectivity. Therefore, this resist could provide an excellent platform to alleviating the challenges of dry etching in future technology nodes.

To improve the resist sensitivity while not losing the pattern resolution, we need to understand the exposure mechanism. To achieve this goal, we have employed our 3D Monte Carlo simulator called 'Excalibur' which allowed us to determine the exposure efficiency of the resist [4, 5]. When designing a new resist it is important to have chemistry that is a source of producing of secondary electrons (SEs). It is well known that these electrons are essential to increasing the resist sensitivity for EBL as they are responsible for exposing the resist [6]. Unfortunately, producing too many SEs will lead to a reduced resolution, therefore a trade-off exists to balance the production of SEs vs resolution. One of the key parameters to achieve this is the density of the resist molecule. It is evident that the mean free path of the electrons can be significantly reduced if the density of the resist is substantially increased as the electrons will experience more collisions due to the reduced distance in between the atoms. This leads to increasing the probability of emitting SEs from the atoms with a high density into the immediate exposure area of the resist film. As stated earlier, the more SEs that are generated means an increase in resist sensitivity but this comes at the expense of resolution. In order to overcome this issue, the resolution can be controlled by increasing the molecular weight or size of the resist molecule. As the molecular weight increases, the fewer positions that the electrons can interact with the resist. This inherently leads to higher resolution patterns because there is only a finite number of molecules that can make up the resist thickness, i.e. the smaller the molecular weight of the resist then more resist molecules are present in the film leading to more scatter interactions. Our resists have a low density and have a very large molecular weight. It can be seen from Figure 1a and b that our resists $[NH_2(CH_2\text{-}CH{=}CH_2)_2][Cr_7NiF_8(O_2C^tBu)_{16}]$ denoted as resist **1**, has a density of ρ = 1.212 g cm^{-3} and has a large molecular weight of 2192 Daltons. Resist **2** is shown in figure 1b and has a molecular formula of $[NH_2(CH_2\text{-}CH{=}CH_2)_2][Cr_7NiF_8(O_2C^tBu)_{15}(O_2CC_5H_4N\text{-}HgCl_2)]$. This resist has a density of ρ = 1.7 g cm^{-3} and has a large molecular weight of 2484 Daltons. These resists have a large hole in the middle, this was designed so that there is more free space than resist matter for the electrons to scatter from, hence, high resolution nano patterns can be produced. For resist **2** we have introduced a dopant in the resist molecule (mercury based compounds) which increases the density at that localized position which means that the incident electrons exposes this area first. This partially renders the entire molecule insoluble in the developing solvent as less electrons are required to produce the pattern. Thus, producing high-resolution patterns while increasing the sensitivity.

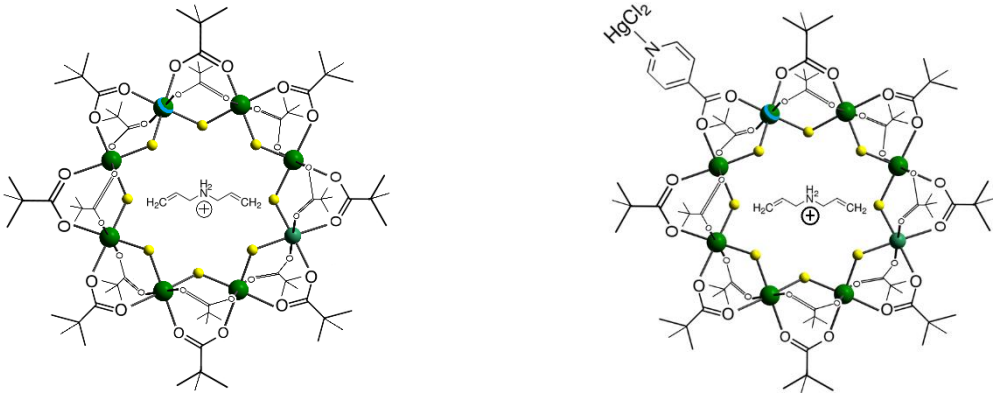

Figure 1. The structures of compounds in the crystal: (a) Resist **1**; (b) Resist **2**;. Cr green, Ni green with a blue band, F yellow, H atoms omitted for clarity.

Of course to function as a EUVL resist, mercury has a larger atomic absorption cross section than any of the atoms present in resist **1**, therefore, we theorized that the mercury dichloride would increase the resist sensitivity because as the EUV radiation ionizes with it, the mercury dichloride would generate low-energy secondary electrons and these SEs will create a chain reaction of cascading electrons that will expose the resist in the immediate exposure area.

We have used our Excalibur Monte Carlo simulator to predict the electron beam lithographic behaviour of both resists. Figure 2 shows a 3D point spread function that illustrates that high resolution nano structures would result for both resists. This is because both resists confine the primary electrons to the immediate write area. By incorporating the

$HgCl_2$ into resist **1** to produce resist **2**, the simulations predicted that further SEs being ejected which would low the exposure dose. It is clear that the primary electrons (PE) will experience more collisions as the effective mean free path is greatly reduced because the $HgCl_2$ increases the density of the resist. The Hg has a larger atomic number any other atoms present in both resists, therefore, this increases the probability of generating an inelastic scattering event is much higher in resist **2**. It was determined from Figure 2 that the Excalibur Monte Carlo simulation calculated that the total number of SEs generated in resist **1** and **2** was 6069 and 9588 respectively. It is evident that resist **2** generated 1.58 times the number of SEs when compared to resist **1**. Therefore, it is expected that resist **2** would be more sensitive to the electron beam than resist **1** by a factor of 1.58.

To perform EBL and EUVL on both resists, both resists were spun coated onto a silicon wafer of 20×20 mm^2. To produce both resist films, 15 mg of each resist was dissolved in 2 g tert butyl methyl ether and each solution was filtered through a 0.2 μm polytetrafluoroethylene syringe filter. Each resist was spin-coated with a spin rate of 6000 rpm for 30 seconds and was followed by a 100 ˚C soft bake for two minutes, resulting with a thickness of 15 nm [2].

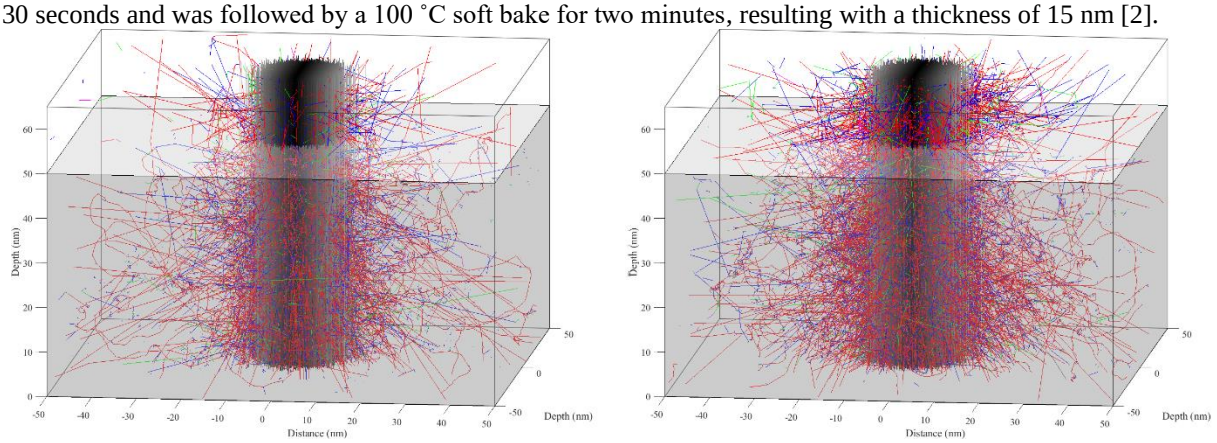

(a) (b)

Figure 2. Point spread function of: (a) Resist **1**; (b) Resist **2**. The acceleration voltage is 30 KeV. The black lines represent the primary electrons from the incident beam while the secondary electrons above 500 eV are represented by the red lines. The secondary electrons which have the associated energies below 500 eV which were generated by first, second and third order collisions are indicated purple, cyan and green. The blue lines are backscattered electrons. 1 million electrons are inserted into a single spot.

The EBL experiments were performed using a FEI Sirion scanning electron microscope. To produce the pattern the electron beam was controlled using Raith ELPHY quantum pattern generator. The energy of the incident electrons was 30 keV. To ascertain the performance of both resists, a pattern was employed that consisted of a one-dimensional matrix of single-pixel-wide lines with 15 nm HP and were 5 μm long. The current and step size used were 50 pA and 4 nm, respectively. The patterns were exposed in sets of 20 lines with one pass of the beam per line, and the line dose of each set ranged from 1000 to 20950 μC/cm^2 with incremental steps of 50 μC/cm^2 and when the pattern was fully resolved this gave the sensitivity of the resist.

The EUVL experiments were performed at the XIL-II beamline at the Swiss Light Source of the Paul Scherer Institute using an EUV interference lithography (EUV-IL) technique [7]. The EUV light was produced by a spatially coherent beam that was tuned at an energy of 92 eV (13.5 nm wavelength) which had a bandwidth of 4%. The photon flux was measured to be 34 mW/cm^2. Both resists were exposed through a photomask which had a pattern of lines and spaces with HP of 16 nm. By varying the exposure time that radiation was incident on the resist, the optimum exposure dose could be determined. The exposure dose ranged from 100 to 2000 mJ/cm^2. After the both lithography techniques were performed on each resist, each resist was developed in hexane for 10 seconds to dissolve away the unexposed resist, then blow-dried with nitrogen.

Figure 3 shows both Monte Carlo simulations and scanning electron microscope (SEM) tilted images of 15 nm HP lines in both resists. At first sight, it is apparent that all of the simulations and the nanostructures in the SEM images appear to be the same. *This was the aim of this investigation*. It is evident that resist **2** requires a significantly reduced exposure dose when compared to resist **1** to fully render each resist insoluble in the developer. It can be seen that when

the resist design rules of large density and large molecular weight are met, the pattern resolution does not change to obtain high-resolution nanostructures. It is important to understand the mechanism to how the features are resolved. To do this we must first determine how far the SE's travel with the resist. We can do this by super imposing the SEs that are generated in the Monte Carlo simulations of Figure 3a and d on the SEM micrograph of Figure 3b and e. It can be seen in Figure 3c and f that SEs create nanostructures by damaging the resist molecule, rendering it insoluble in the developing solvent. Looking at Figures 3c and f, it appears that the first order SEs (red) play the most dominate role, but it's the second order SEs have the most effect because the number of first order SE is 19170 and 21066 in resist **1** and **2** respectively whereas the number of second order SEs is 31456 and 39066 in resist **1** and **2** respectively. What is happening here is that the first order SEs masks the concentration of second order SEs and these electron's travel less than 10 nm.

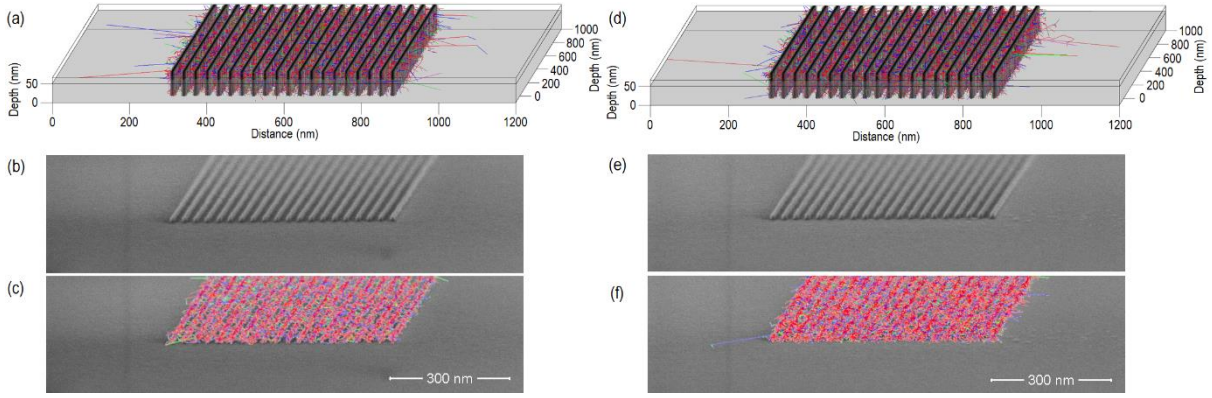

Figure 3. The internal electron scattering interactions inside 15 nm half pitch lines simulated in: a) Resist **1** using 30 KeV acceleration voltage with 18750 incident electrons per spot; b) Scanning electron micrographs of developed patterns of 15 nm half pitch lines fabricated in resist **1** using 30 KeV acceleration voltage requiring a dose of 7500 μC cm^{-2}; c) Monte Carlo simulation of SEs that are superimposed on the developed pattern that is shown in (b); d) Resist **2** using 30 KeV acceleration voltage with 11800 incident electrons per spot; e) Scanning electron micrographs of developed patterns of 15 nm half pitch lines fabricated in resist **2** using 30 KeV acceleration voltage requiring a dose of 4700 μC cm^{-2}; f) Monte Carlo simulation of SEs that are superimposed on the developed pattern that is shown in (e).

Even though both resists achieved a resolution of 15 nm half pitch with good uniformity. It was ascertained that the sensitivity of both resists is considerably different where resist **1** and **2** gave sensitivities of 7500 and 4700 μC cm^{-2} respectively. Therefore, resist **2** is more sensitive than resist **1** by a factor of 1.6, which is in agreement with the Excalibur Monte Carlo simulation shown in Figure 2.

The SEM images in Figure 4 show nanopatterns produced using the EUVL technique. In both resist cases, they have achieved a resolution of 16 nm HP. Just like the EBL experiments all of the patterns appear to be the same. To produce a pattern with a HP of 16 nm, it was determined that the dose required to expose resists **1** and **2** was 625 and 322 mJ/cm^2 respectively. Again, resist **2** is more sensitive than resist **1** by a factor of 1.94. Figure 4a shows bridging between the lines this is due to that the exposure latitude of the resist. When the EUVL experiment was performed the exposure dose was on the high end of the dose scale.

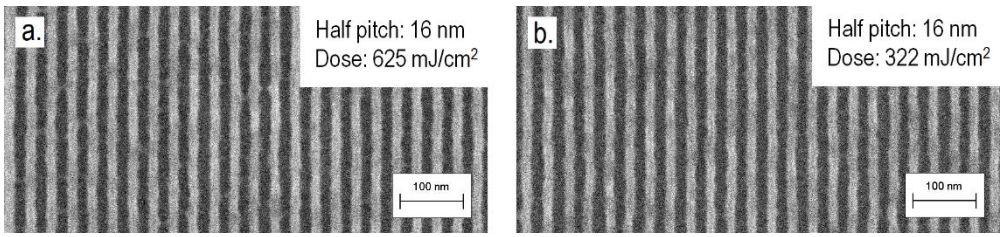

Figure 4. a) Scanning electron micrograph of patterns of 16 nm hp lines fabricated in Resist **1**; b) in Resist **2**.

Building upon Figures 3 and 4, Figure 5a shows the exposure doses required to produce the patterns from the EBL and EUVL experiments. In both lithographic techniques (EBL and EUVL), the exposure dose was decreased by the presence of $HgCl_2$, this demonstrates that we have chemical control of the exposure dose. The immediate observation

from Figure 5b is that in the EBL experiment, the exposure dose needed for resist **2** decreases by a factor of 1.6 times when compared to **1** for the 15 nm HP, respectively. This matches the Monte Carlo simulations of Figure 2, which was 1.58.

For the EUVL experiment, the exposure dose that was required for resist **2** is reduced by a factor of 1.94 times when compared to resist **1** for the 16 nm HP, respectively. This is due to that resist **2** has $HgCl_2$ bound to the outside of the molecule. The atomic absorption cross-section associated with mercury is the strongest of all of the elements present in the resist **1** and **2**. The exposing mechanism is based upon the metals present in the resist, where they absorb the EUV radiation and emit low energy SEs into the immediate exposure area. These SEs will collide with the pivalates on the outside of the molecule and cause a cascade of SEs which decomposes the pivalate part of the resist molecule rendering it partially insoluble in the developing solvent and has the effect of reducing the exposure dose while maintaining resolution [8]. Comparing this with resist **1**, There is no mercury present in resist **1** and solely relies upon the atomic absorption cross section of Chromium. The exposing mechanism is based upon the chromium present in the resist, where they absorb the EUV radiation and emit low energy SEs into the immediate exposure area and decompose the pivalate part of the resist molecule. The mercury atomic absorption cross-section is 2.6 times larger than that of the chromium atomic absorption cross-section [9]. However, it must be pointed out that there is more chromium atoms in the resist than mercury. Therefore, it was not expected that the resist sensitivity gain will be as high 2.6, but that being said, mercury has more electrons in its outer shells than the chromium atom has, thus the probability of striking the electrons in these shells is larger and producing SEs.

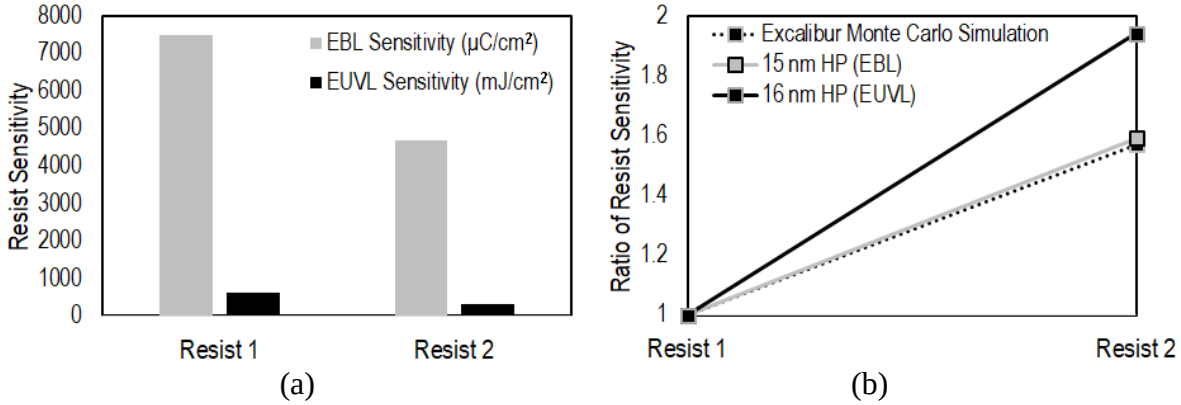

Figure 5. a) Dose-to-clear values for all resist materials using EUVL and EBL. b) Relative of the sensitivity of the resists for EUVL and EBL.

To further explore the exposure mechanism of both resists **1** and **2**, X-ray photoelectron spectroscopy (XPS) was employed to image the resist in situ before and after exposure to the electron beam. Figure 6 shows the X-ray photoelectron spectra (XPS) of resist **2** before and after electron beam exposure. Resist 2 was chosen for the XPS exposure mechanism experiment because it has all of the elements present. For clarity the spectra has been normalized with respect to the Carbon 1S peak. Looking at the Carbon 1S peak; even though the main Carbon peak appears to be unchanged it can be seen that the side peak which represents the acetate O – C = O part of the pivalate has been considerably reduced after exposure to the electron beam. It is clear, that the electron beam decomposes the carboxylates to form carbon dioxide (CO_2) or/and carbon monoxide (CO) products [10]. These gases are diffusing out of the film into the vacuum. This inherently leaves the chromium and fluorine atoms of the main ring like structure behind on the silicon substrate. Consequently, this changes the solubility of the resist. Where this product is not soluble in the developer which in our case is Hexane. Figure 6 shows the Cr 2p peak before and after the electron beam exposure. It is evident that the chromium 2p peak has broadened and has shifted to the right. This means that the chromium has changed from a single oxidation state to a mixture of states which suggests it is being reduced away towards a mixture of CrO_xF_y compounds [10].

These products are also not be soluble in hexane. It can be seen that after exposure, the Cr 2p peak increases by a factor 2 while the O 1S peak decreases by 30%. Figure 6 shows the Ni 2p peak and it is clear that its shape and intensity have not changed after the electron beam exposure, but it has shifted right. This means that has transformed into a more metal oxide by changing from a single oxidation to a mixture of states to produce a NiO_xF_y compounds [10].

Again, these products are not soluble in Hexane. Before exposure the mercury peaks are clearly visible and after exposure they have disappeared. This is due to that upon exposure the mercury emits a SE and becomes dissociated from the main molecule. Then it sublimes from the film this is because its vapour pressure is very low.

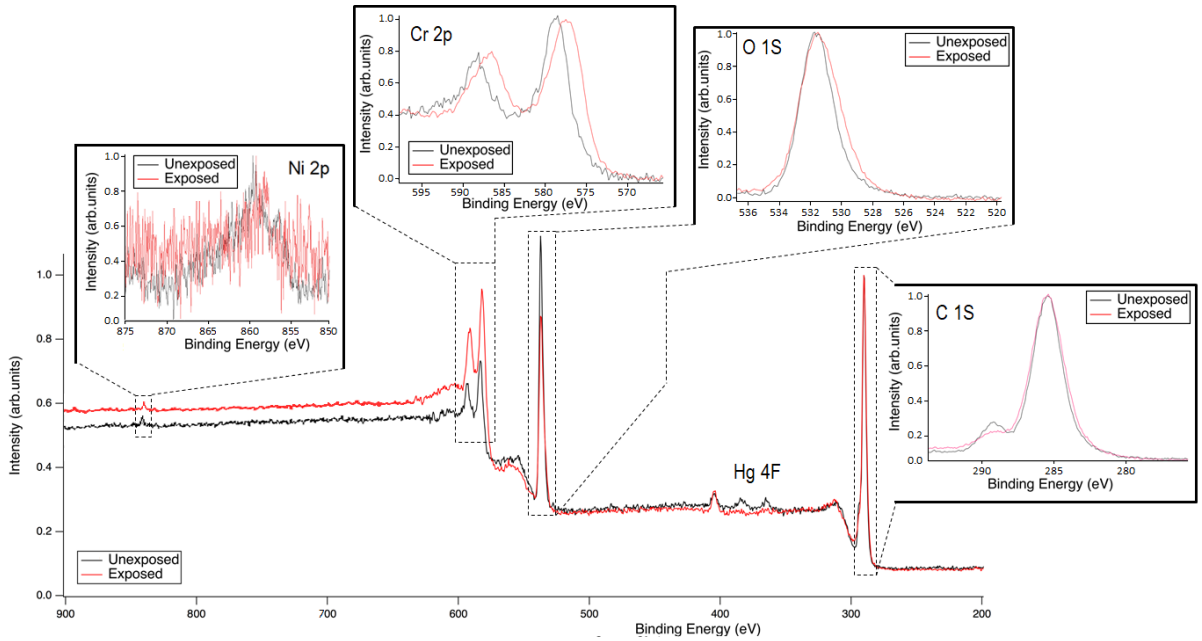

Figure 6. X-ray photoelectron spectra of resist **2** material before and after exposure to the electron beam.

Figure 7 shows the entire silicon dry etching process of resist **1** and **2**. Figure 7a and d shows 15 nm HP lines that have been patterned with the 30 keV electron beam into resist **1** and **2** respectively. A Pseudo Bosch process that uses inductively coupled plasma (ICP) of SF_6 and C_4F_8 gases was employed to etch the underlying silicon (Figure 7b and e).

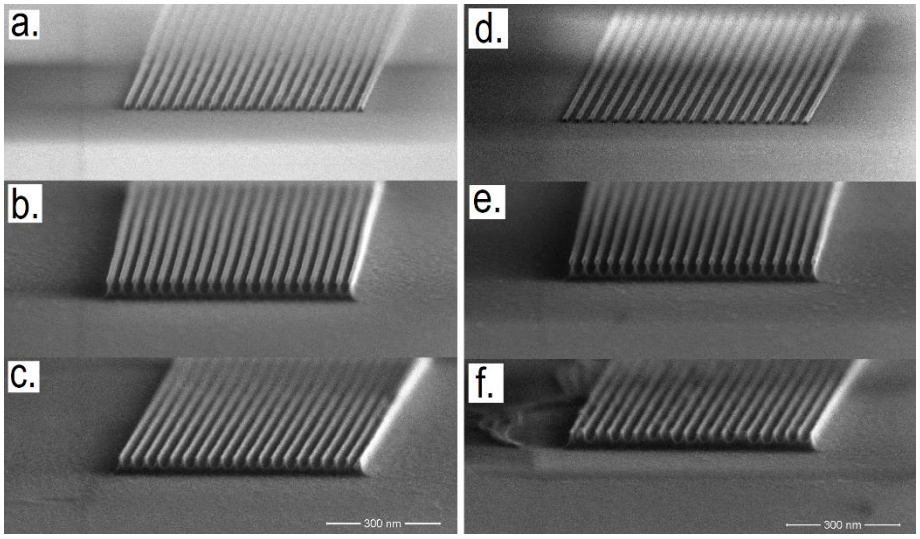

Figure 7. The etch process in resists **1**, **2** (a) Patterned resist **1** before the dry etching process, (b) resist **1** after a 18 second pBosch dry etch process, (c) Fins with a 8 nm width after removal of resist **1**. (d) Patterned resist **2** before the dry etching process, (e) resist **2** after a 18 second pBosch dry etch process, (f) Fins with a 8 nm width after removal of resist **2**. The parameters of the process were gases: SF_6 and C_4F_8 with flow rates of 22 and 35 sccm respectively, the DRIE forward power was 20 W and the ICP forward power was 1200 W.

After the etching step, the resolution of the silicon nanostructures was 9 nm and exhibited a height of 14.6 nm (Figure 7c and f) and the remaining resist thicknesses of resist **1** and **2** was measured to be 14.2 nm. Giving rise to a resist etch rate of 0.022 nm s^{-1}. The silicon depth was measured to be 24 nm giving an etch rate of 1.33 nm s^{-1}. Therefore, the etch selectivity of resists **1** and **2** is 60:1 with respect to silicon. Both resists **1** and **2** have demonstrated extremely high dry etch selectivity when compared with silicon, this is because the CrO_xF_y and NiO_xF_y compounds are not reactive to chemical dry SF_6 and C_4F_8 etching. The dry etch selectivity seen here is approximately the equivalent selectivity that is achieved with aluminum oxide masks [11]. To our knowledge these are the best etch masks available. Unfortunately, they require more processing steps compared with our process. Other high resolution resists such as PMMA, ZEP520A and HSQ have etch selectivities of only 2:1, 2.9:1 and 4.2:1 respectively [12]. Considering the HSQ resist case, the resist materials presented here out perform this resist by a factor of approximately 14.

CONCLUSION

Two metal-organic negative tone resists have been investigated by EBL and EUVL. We have demonstrated that both resist **1** and **2** have achieved a resolution of 15 and 16 nm HP by EBL and EUVL respectively. It was determined that the exposure sensitivity of resist **2** when compared to resist **1** was increased by a factor of 1.6 and 1.94 times for the EBL and EUVL studies by chemical design of introducing mercury dichloride into resist **2** while maintaining a high resolution of 15 and 16 nm HP, respectively. The EBL experimental date showed excellent agreement with the Monte Carlo simulations, and suggest that the improvement in sensitivity is due to an increase in density which generates SEs within the resist within the immediate exposure area. Preliminary studies show that both resists **1** and **2** have an excellent etch performance of a 60:1 dry etch selectivity, which we conclude is due to the presence of CrO_xF_y and NiO_xF_y which are not reactive in an SF_6 and C_4F_8 plasma.

ACKNOWLEDGEMENTS

This work was supported by the EPSRC(UK) (EP/P000444/1 and EP/R023158/1) including an Established Career Fellowship to R. E. P. W. (EP/R011079/1) and by an Innovate UK award (Project Number 18238). The authors gratefully acknowledge critical support and infrastructure provided for this work by the Kavli Nanoscience Institute at Caltech. This project has received funding from the EU-H2020 research and innovation program under grant agreement No. 654360 having benefitted from the access provided by PSI in Villigen within the framework of the Nanoscience Foundries and Fine Analysis Europe Transnational Access Activity.

REFERENCES

[1] 'More Moore', IEEE International Roadmap for Devices and Systems, 2018. www.irds.ieee.org. Accessed 03/02/2020.
[2] Lewis, S.; DeRose, G.; Hunt, M.; Scherer, A.; Yeates, S.; Winpenny, R. E. P.; Alty, H. R.; Werthiem, A.; Li, J.; Fowler, T.; et al. Design and Implementation of the next Generation Electron Beam Resists for the Production of EUVL Photomasks. In *Photomask Technology 2018*; Rankin, J. H., Gallagher, E. E., Eds.; SPIE: Monterey, United States, **2018**, 108100N. https://doi.org/10.1117/12.2501808.
[3] Lewis, S. M.; Hunt, M. S.; DeRose, G. A.; Alty, H. R.; Li, J.; Wertheim, A.; De Rose, L.; Timco, G. A.; Scherer, A.; Yeates, S. G.; Winpenny, R. E. P. Plasma-etched pattern transfer of sub-10 nm structures using a metal-organic resist and helium ion beam lithography. *Nano Lett*. **2019**, *19*, 6043−6048.
[4] Lewis, S. M.; DeRose. G. A. in Frontiers of Nanoscience, Materials and Processes for Next Generation Lithography: SML electron beam resist: ultra-high aspect ratio nanolithography; Elsevier, 2016, 11, pp 421 – 446.
[5] Lewis, S.M.; Fernandez, A.; DeRose, G.A.; Hunt, M.S.; Whitehead, G.F.; Lagzda, A.; Alty, H.R.; Ferrando-Soria, J.; Varey, S.; Kostopoulos, A.K.; Schedin, F.; Winpenny, R. E. P. Use of supramolecular assemblies as lithographic resists. *Angewandte Chemie.* **2017**, 129(24), 6853-6856. https://doi.org/10.1002/anie.201700224.
[6] Wu, B.; Neureuther, A.R. Energy deposition and transfer in electron-beam lithography. Journal of Vacuum Science & Technology B: Microelectronics and Nanometer Structures Processing, Measurement, and Phenomena 19, 2508 (**2001**); https://doi.org/10.1116/1.1421548.

[7] Popescu, C.; Frommhold, A.; McClelland, A.; Roth, J.; Ekinci, Y.; Robinson, A. P. G.; Sensitivity enhancement of the high resolution xMT multi-trigger resist for EUV lithography, Proc. SPIE 10143, Extreme Ultraviolet (EUV) Lithography VIII, 101430V (**2017**); https://doi.org/10.1117/12.2258098.
[8] Lewis, S. M,; Alty, H. R.; Vockenhuber, M.; DeRose, G. A.; Fernandez, A.; Kazazis, D.; Winpenny, P. L.; Grindell, R.; Timco, G. A.; Scherer, A.; Ekinci, Y.; Winpenny, R. E. P.; Sensitivity enhancement of a high-resolution negative-tone nonchemically amplified metal organic photoresist for extreme ultraviolet lithography, J. Micro/Nanopattern. Mats. Metro. 21(4) 041404 (**2022**) https://doi.org/10.1117/1.JMM.21.4.041404
[9] Fallica, R.; Haitjema, J.; Wu, L.; Ortega, S. C.; Brouer, A. M.; Ekinci, Y. Absorption coefficient of metal containing photoresists in the extreme ultraviolet. J. Micro/Nanolithography, MEMS and MOEMS. 17 (2) 023505 (**2018**). https://doi.org/10.1117/1.JMM.17.2.023505.
[10] Lewis, S. M.; DeRose, G. A.; Alty, H. R.; Hunt, M. S.; Lee, N.; Mann, J. A.; Grindell, R.; Wertheim, A.; De Rose, L.; Fernandez, A.; and Muryn, C. A.; Whitehead, G. F. S.; Timco, G. A.; Scherer, A.; Winpenny, R. E. P. Tuning the Performance of Negative Tone Electron Beam Resists for the Next Generation Lithography. Advanced Functional Materials, 32 (32). **2022**. https://doi:10.1002/adfm.202202710.
[11] Henry, D. S.; Walavalkar, S.; Homyk, A.; Scherer, A.; *Nanotechnology*, **2009**, *20*, 255305.
[12] Goodyear, A.; Boettcher, M.; Stolberg, I.; Cooke, M.; *Proc. SPIE* **2015**, *9428*, 94280V.